Inorg. Chem. **2008**, *47*, 8437−8443

Forum

Optical Properties of Cation-Substituted Zinc Oxide

Young-Il Kim*,† and Ram Seshadri†,‡

Materials Department and Materials Research Laboratory and Department of Chemistry and Biochemistry, University of California, Santa Barbara, California 93106

Received May 19, 2008

Zinc oxide (ZnO)-based optoelectronics has emerged as a frontier area in semiconductor research in recent years. In the design of ZnO-based optoelectronic devices, cation-substituted ZnO serves as essential components for the desired device functions. Band-gap engineering by cation substitution enables the facile preparation of barrier layers and quantum wells in device structures. Wurtzite solid solutions $Zn_{1-x}Mg_xO$, $Zn_{1-x}Cd_xO$, and $Zn_{1-x}Be_xO$ have been reported as examples where band gaps are gradually modulated as functions of x. In this contribution, we present an overview of composition-dependent band-gap variations of $Zn_{1-x}M_xO$ solid solutions. In addition, we describe the optical properties and microstructural evolution in polycrystalline $Zn_{1-x}Mg_xO$ ($0 \leq x \leq 0.15$). It is proposed that chemical strain associated with cation substitution has an impact on the band-gap magnitude, crystallite morphology, and optical defects.

Introduction

Zinc oxide (ZnO) possesses unique electrical and chemical properties that have found a wide range of applications in piezoelectrics, varistors, catalysts, pigments, etc.[1,2] However, modern-day uses of ZnO are being extended in increasingly sophisticated ways where the emphasis is on the magnetic, optical, and electronic properties of the pure and doped/substituted compounds.[3,4] One example of an application that has received great attention are diluted magnetic semiconductors and their applications to spin-based electronics (so-called spintronics).[5,6] The realization of magnetic semiconductors with high ordering temperatures, meaning near or above room temperature, opens up the possibility of practical spin transistors, ultradense nonvolatile semiconductor memory, and spin-polarized optical emitters.[5,6] Following theoretical analysis by Dietl et al.,[7] which predicted room temperature ferromagnetism in heavily hole-doped $Zn_{0.95}Mn_{0.05}O$, there has been a great deal of research effort dedicated to ZnO-based magnetic systems,[8–13] not all of it necessarily sound.

Another important area in current ZnO research is in optoelectronics. At room temperature, ZnO has a band gap of 3.3 eV[14] and an exciton binding energy of 60 meV ($\approx 2.4k_BT$),[15] with the latter, in particular, indicative of a potential for superior lasing and light-emitting behavior.[16] From the material processing viewpoint, ZnO has additional

* To whom correspondence should be addressed. E-mail: ykim@mrl.ucsb.edu.
† Materials Department and Materials Research Laboratory.
‡ Department of Chemistry and Biochemistry.

(1) Ozgur, U.; Alivov, Ya. I.; Liu, C.; Teke, A.; Reshchikov, M. A.; Dogan, S.; Avrutin, V.; Cho, S.-J.; Morkoc, H. *J. Appl. Phys.* **2005**, *98*, 041301.
(2) Pearton, S. J.; Norton, D. P.; Ip, K.; Heo, Y. W.; Steiner, T. *J. Vac. Sci. Technol. B* **2004**, *22*, 932.
(3) Wolf, S. A.; Awschalom, D. D.; Buhrman, R. A.; Daughton, J. M.; von Molnar, S.; Roukes, M. L.; Chtchelkanova, A. Y.; Treger, D. M. *Science* **2001**, *294*, 1488.
(4) Tsukazaki, A.; Ohtomo, A.; Kita, T.; Ohno, Y.; Ohno, H.; Kawasaki, M. *Science* **2007**, *315*, 1388.
(5) Prinz, G. A. *Science* **1998**, *282*, 1660.
(6) Liu, C.; Yun, F.; Morkoc, H. *J. Mater. Sci.* **2005**, *16*, 555.
(7) Dietl, T.; Ohno, H.; Matsukura, F.; Cibert, J.; Ferrand, D. *Science* **2000**, *287*, 1019.
(8) Sharma, P.; Gupta, A.; Rao, K. V.; Owens, F. J.; Sharma, R.; Ahuja, R.; Guillen, J. M. O.; Johansson, B.; Gehring, G. A. *Nat. Mater.* **2003**, *2*, 673.
(9) Ueda, K.; Tabata, H.; Kawai, T. *Appl. Phys. Lett.* **2001**, *79*, 988.
(10) Lawes, G.; Risbud, A. S.; Ramirez, A. P.; Seshadri, R. *Phys. Rev. B* **2005**, *71*, 045201.
(11) Han, S.-J.; Jang, T.-H.; Kim, Y. B.; Park, B.-G.; Park, J.-H.; Jeong, Y.-H. *Appl. Phys. Lett.* **2003**, *83*, 920.
(12) Risbud, A. S.; Spaldin, N. A.; Chen, Z. Q.; Stemmer, S.; Seshadri, R. *Phys. Rev. B* **2003**, *68*, 205202.
(13) Seshadri, R. *Curr. Opin. Solid State Mater. Sci.* **2005**, *9*, 1.
(14) Srikant, V.; Clarke, D. R. *J. Appl. Phys.* **1998**, *83*, 5447.
(15) Hummer, K. *Phys. Status Solidi* **1973**, *56*, 249.
(16) Look, D. C. *Mater. Sci. Eng., B* **2001**, *80*, 383.

10.1021/ic800916a CCC: $40.75
Published on Web 09/29/2008

advantages over other wide-gap semiconductors: availability of large and high-quality single-crystal substrates, stability to high-energy radiation, and amenability to wet-chemical etching, all of which have helped to stimulate the renewed interest in ZnO as a semiconductor material.[2] It should be mentioned, however, that the crucial goal of p-type ZnO remains tantalizingly out of reach. As part of numerous efforts, cation substitution of ZnO has been used as a means of band-gap engineering and constitutes an important step for creating barrier layers and quantum wells in device heterostructures.[17–19] Recent experimental studies have shown that the optical band gap of ZnO can be widely tuned by alloying with MO (M = Be, Mg, and Cd).[17–22] Band-gap engineering studies on $Zn_{1-x}Mg_xO$ and $Zn_{1-x}Cd_xO$ have previously been reviewed in an exhaustive manner.[1] In the present study, we aim at finding a universal trend of composition-dependent band-gap variations in $Zn_{1-x}M_xO$, using the representative experimental results on $Zn_{1-x}Mg_xO$ and $Zn_{1-x}Cd_xO$ as well as the newly reported results on $Zn_{1-x}Be_xO$. From the comparison of band-gap variations by different substituent cations, we suggest that the band gaps of $Zn_{1-x}M_xO$ correlate well with the size and electronegativity of the cation M as well as the substitution level x.

Cation substitution for band-gap engineering is distinguished from conventional doping studies of ZnO. While the latter, using aliovalent substituents (e.g., Li^+, Al^{3+}, Ga^{3+}, F^-, N^{3-}), are intended to modify the carrier type and density, the former employ isovalent substituents as listed above. In general, the substitution level is significantly high in isovalent substitutions, often resulting in considerable structural change. Therefore, the optical properties of $Zn_{1-x}M_xO$, where M is divalent, can be better understood by taking into account the macroscopic and microscopic structural aspects of a solid solution. For the example of $Zn_{1-x}Mg_xO$, we examine the effects of cation substitution on the structural and optical defects. In recent synchrotron X-ray diffraction and Raman studies on polycrystalline $Zn_{1-x}Mg_xO$, we have shown that Mg substitution causes c-axis compression of the hexagonal wurtzite lattice and also that Mg and Zn have distinct tetrahedral coordination geometries in the $Zn_{1-x}Mg_xO$.[21,22] In this contribution, we focus on the defect nature of polycrystalline samples by employing diffuse-reflectance absorption spectroscopy, photoluminescence (PL) measurements, and X-ray line-broadening size-strain analysis.

Preparations of $Zn_{1-x}M_xO$ (M = Be, Mg, and Cd). Cation substitution of ZnO has been extensively studied, for various purposes such as magnetic semiconductors and transparent conductors.[1,2,6] The three systems $Zn_{1-x}M_xO$ (M = Be, Mg, and Cd) are known as successful examples of systematic band-gap engineering. Among them, $Zn_{1-x}Mg_xO$ is by far the most studied. As reported in the literature, the $Zn_{1-x}Mg_xO$ samples have been prepared in various ways, including (i) thin films by pulsed-laser deposition,[17] radical source molecular beam epitaxy,[23] metal−organic vapor-phase epitaxy,[24] radio-frequency magnetron sputtering,[25] spray pyrolysis,[26] and dip coating,[27] (ii) polycrystalline powders by high-temperature solid-state reaction[28] and coprecipitate decomposition,[21] (iii) nanostructures by a solution route,[29] and (iv) single crystals by hydrothermal reaction.[30] $Zn_{1-x}Cd_xO$ samples have been prepared in the thin films by pulsed-laser deposition,[18] metal−organic vapor-phase epitaxy,[31] reactive magnetron sputtering,[32] radical source molecular beam epitaxy,[33] spray pyrolysis,[34] and sol−gel spin coating[35] and in the polycrystalline powder by high-temperature reaction.[36] Only a few reports on the $Zn_{1-x}Be_xO$ system are to be found, for example, prepared by hybrid beam deposition.[19]

It is noteworthy that thin film and polycrystalline samples of the above solid solutions can have different characteristics of compositional distribution and phase stability. Because thin-film growth processes are substantially affected by kinetic parameters, the solubility range of as-prepared thin films appears significantly wider than that in the polycrystalline phases. For example, thin films of $Zn_{1-x}Mg_xO$ could be deposited up to $x = 0.33$ without segregation of the MgO phase,[17] but an annealing study revealed a solubility limit at $x \approx 0.15$.[37] In polycrystalline $Zn_{1-x}Mg_xO$ prepared at 550 and 1200 °C, the solubility limits were observed to be 15% and 16%, respectively.[21,38] $Zn_{1-x}Cd_xO$ and $Zn_{1-x}Be_xO$ thin-film systems showed similar trends, where the solubility limits are lowered in thermodynamic conditions.[39,40] The studies indicate that phase equilibration of these solid solutions requires sufficiently long annealing times under

(17) Ohtomo, A.; Kawasaki, M.; Koida, T.; Masubuchi, K.; Koinuma, H.; Sakurai, Y.; Yoshida, Y.; Yasuda, T.; Segawa, Y. *Appl. Phys. Lett.* **1998**, *72*, 2466.
(18) Makino, T.; Tuan, N. T.; Segawa, Y.; Chia, C. H.; Kawasaki, M.; Ohtomo, A.; Tamura, K.; Koinuma, H. *Appl. Phys. Lett.* **2000**, *77*, 1632.
(19) Ryu, Y.; Lee, T.-S.; Lubguban, J. A.; Corman, A. B.; White, H. W.; Leem, J. H.; Han, M. S.; Park, Y. S.; Yoon, C. J.; Kim, W. J. *Appl. Phys. Lett.* **2006**, *88*, 052103.
(20) Choopun, S.; Vispute, R. D.; Yang, W.; Sharma, R. P.; Venkatesan, T.; Shen, H. *Appl. Phys. Lett.* **2002**, *80*, 1529.
(21) Kim, Y.-I.; Page, K.; Seshadri, R. *Appl. Phys. Lett.* **2007**, *90*, 101904.
(22) Kim, Y.-I.; Page, K.; Limarga, A. M.; Clarke, D. R.; Seshadri, R. *Phys. Rev. B* **2007**, *76*, 115204.
(23) Tampo, H.; Shibata, H.; Maejima, K.; Yamada, A.; Matsubara, K.; Fons, P.; Niki, S.; Tainaka, T.; Chiba, Y.; Kanie, H. *Appl. Phys. Lett.* **2007**, *91*, 261907.
(24) Park, W. I.; Yi, G.-C.; Jang, H. M. *Appl. Phys. Lett.* **2001**, *79*, 2022.
(25) Choi, C.-H.; Kim, S.-H. *J. Cryst. Growth* **2005**, *283*, 170.
(26) Zhang, X.; Li, X. M.; Chen, T. L.; Zhang, C. Y.; Yu, W. D. *Appl. Phys. Lett.* **2005**, *87*, 092101.
(27) Ghosh, R.; Basak, D. *Appl. Phys. Lett.* **2007**, *101*, 023507.
(28) Zhang, J.; Pan, F.; Hao, W.; Wang, T. *Mater. Sci. Eng., B* **2006**, *129*, 93.
(29) Peng, W. Q.; Qu, S. C.; Cong, G. W.; Wang, Z. G. *Appl. Phys. Lett.* **2006**, *88*, 101902.
(30) Wang, B.; Callahan, M. J.; Bouthillette, L. O. *Cryst. Growth Des.* **2006**, *6*, 1256.
(31) Gruber, Th.; Kirchner, C.; Kling, R.; Reuss, F.; Waag, A.; Bertram, F.; Forster, D.; Christen, J.; Schreck, M. *Appl. Phys. Lett.* **2003**, *83*, 3290.
(32) Ma, D. W.; Ye, Z. Z.; Chen, L. L. *Phys. Status Solidi A* **2004**, *201*, 2929.
(33) Sakurai, K.; Takagi, T.; Kubo, T.; Kajita, D.; Tanabe, T.; Takasu, H.; Fujita, S; Fujita, S *J. Cryst. Growth* **2002**, *237–239*, 514.
(34) Vigil, O.; Vaillant, L.; Cruz, F.; Santana, G.; Morales-Acevedo, A.; Contreas-Puente, G. *Thin Solid Films* **2002**, *361–362*, 53.
(35) Choi, Y. S.; Lee, C. G.; Cho, S. M. *Thin Solid Films* **1996**, *153*, 289.
(36) Mohanta, A.; Thareja, R. K. *J. Appl. Phys.* **2008**, *103*, 024901.
(37) Ohtomo, A.; Shiroki, R.; Ohkubo, I.; Koinuma, H.; Kawasaki, M. *Appl. Phys. Lett.* **1999**, *27*, 4088.
(38) Sapozhnikov, Yu. P.; Kondrashev, Yu. D.; Markovskii, L. Ya.; Omel'chenko, Yu. A. *Russ. J. Inorg. Chem.* **1961**, *6*, 1289.

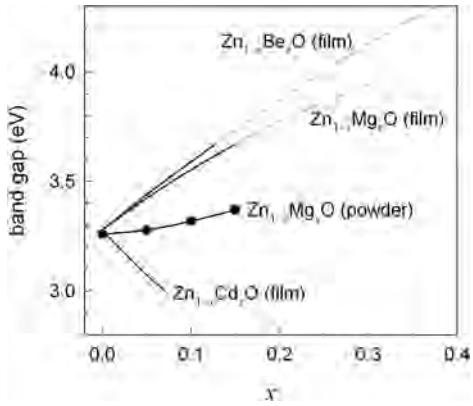

Figure 1. Band-gap energy variation in the ternary alloys $Zn_{1-x}M_xO$ (M = Mg, Cd, and Be). Data are from refs 17– 22, 37, 39 and 40. Experimental data for the metastable $Zn_{1-x}Be_xO$ and $Zn_{1-x}Mg_xO$ thin-film phases are represented by gray dashed lines.

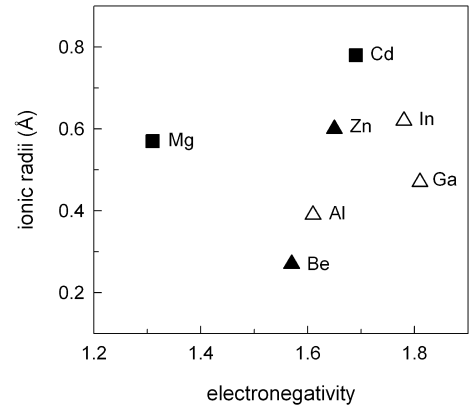

Figure 2. Four-coordinate ionic radii and Pauling electronegativity of cations in II−VI oxides (filled symbols) and III−V nitrides (open symbols). Triangles and squares denote respectively the wurtzite and rock salt crystal systems of the binary oxides and nitrides.

appropriate thermal conditions. Further implied is that the local compositional fluctuations and/or the metastable phases have to be taken into account when interpreting the physical properties exhibited by the as-prepared thin films of the solid solutions.

Optical Properties of $Zn_{1-x}M_xO$ (M = Be, Mg, and Cd). The band-gap energies (E_g) of II−VI or III−V semiconductors can be systematically modulated by substitution with congener cations. For GaN and GaAs, substitution studies using Al and In have been extensively performed,[41,42] and in these substitutional cases, the solid solution limit is 100% because the end members are isostructural. In the case of ZnO, the ternary alloys $Zn_{1-x}M_xO$ (M = Be, Mg, and Cd) are known to form wurtzite-type solid solutions with finite upper limits of x.[37,39,40] In any of the above $Zn_{1-x}M_xO$ systems, the solid solution does not form in the entire x range due to geometric incompatibility. In contrast to the tetrahedral ZnO lattice, both MgO and CdO favor the octahedral rock salt structure. On the other hand, BeO is isostructural to ZnO but the sizes of Be^{2+} (r = 0.27 Å) and Zn^{2+} (r = 0.60 Å) are very different. Under thermodynamic conditions, the solubility limits of the above solid solutions are estimated as 15%, 13%, and 7% respectively for Mg, Be, and Cd substitutions.[37,39,40] However, within the solid solution range, the band-gap energy monotonically changes as a function of x without saturation. Figure 1 shows the band-gap energies of $Zn_{1-x}M_xO$ (M = Be, Mg, and Cd) as compiled from previous studies using thin-film and powder specimens.[17–22,37,39,40] The band-gap shift in each solid solution is consistent with the band-gap values of end-member binary oxides. With ZnO (E_g = 3.3 eV)[14] taken as the parent semiconductor, alloying with CdO (E_g = 2.2 eV)[43] narrows the band gap whereas alloying with insulators MgO (E_g = 7.8 eV)[44] or BeO (E_g = 10.6 eV)[45] widens the gap. As a result, the band-gap values of wurtzite $Zn_{1-x}M_xO$ can be tuned in a range as wide as 0.7 eV (3.0−3.7 eV).

Although the electronic perturbation of the cation substitution is assumed to be the primary origin of the band-gap change in $Zn_{1-x}M_xO$, it cannot solely account for the observed results. As shown in Figure 2, the Pauling electronegativity (χ)[46] increases in the order χ(Mg) < χ(Be) < χ(Zn) < χ(Cd), suggesting that the band gap would change and increase more steeply with x in $Zn_{1-x}Mg_xO$ than in $Zn_{1-x}Be_xO$. However, the observed trend in Figure 1 contradicts this suggestion. Similarly for the III−V nitrides, the cation electronegativity does not correlate with the band gaps of pure or alloyed nitride compounds. While the electronegativity increases as χ(Al) < χ(In) < χ(Ga), the band-gap magnitudes are in the order E_g(InN) < E_g(GaN) < E_g(AlN), with those of $Ga_{1-x}In_xN$ and $Ga_{1-x}Al_xN$ intervening between the alloy end members'.[41] It is therefore implied that additional factors such as geometric ones play a significant role in the band-gap variation of the $Zn_{1-x}M_xO$ and $Ga_{1-x}M_xN$ systems. In Figure 2, we compare the ionic radii[47] of the cation components of the above II−VI oxides and III−V nitrides and find that the ion size can be a more useful parameter than the electronegativity for estimating the band gap of the respective compound semiconductor. In a qualitative manner, it can be stated that the band gap of a II−VI or III−V semiconductor decreases when the cations become larger and more electronegative. Presumably, the ion size has an immediate influence on the interactions between the cation and anion frontier orbitals. Within the given wurtzite crystal system, the larger cation size will facilitate covalency with anion 2p orbitals, broaden the valence and conduction bands, and therefore narrow the band gap.

Band-gap variations of thin-film and polycrystalline $Zn_{1-x}Mg_xO$ are separately displayed in Figure 1. Both of them indicate an increase of the band gap with x, but the dependences are quite different. Because the compositions of both types of samples have been determined in fairly

(39) Makino, T.; Segawa, Y.; Kawasaki, M.; Ohtomo, A.; Shiroki, R.; Tamura, K.; Yasuda, T.; Koinuma, H. *Appl. Phys. Lett.* **2001**, *78*, 1237.
(40) Kim, W. J.; Leem, J. H.; Han, M. S.; Park, I.-W.; Ryu, Y. R.; Lee, T. S. *J. Appl. Phys.* **2006**, *99*, 096104.
(41) Strite, S.; Morkoc, H. *J. Vac. Sci. Technol. B* **1992**, *10*, 1237.
(42) Chua, S. J.; Ramam, A. *J. Appl. Phys.* **1996**, *80*, 4604.
(43) Ueda, N.; Maeda, H.; Hosono, H.; Kawazoe, H. *J. Appl. Phys.* **1998**, *84*, 6174.
(44) Roessler, D. M.; Walker, W. C. *Phys. Rev. B* **1967**, *159*, 733.
(45) Roessler, D. M.; Walker, W. C.; Loh, E. *J. Phys. Chem. Solids* **1969**, *30*, 157.
(46) Allred, A. L. *J. Inorg. Nucl. Chem.* **1961**, *17*, 215.
(47) Shannon, R. D. *Acta Crystallogr., Sect. A* **1976**, *14*, 235.

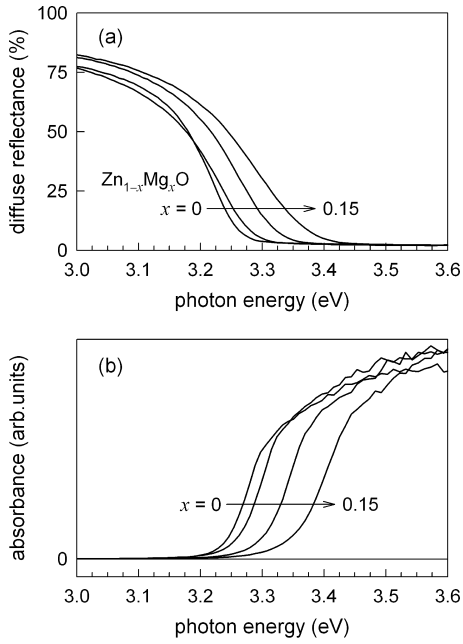

Figure 3. (a) Diffuse-reflectance spectra of polycrystalline $Zn_{1-x}Mg_xO$ (x = 0, 0.05, 0.10, and 0.15) and (b) the corresponding Kubelka−Munk functions.

reliable ways, Rietveld refinement for polycrystalline samples[21] and inductively coupled plasma optical emission spectroscopy for thin films,[17] the discrepancy seems to arise rather from extrinsic factors. One possible reason is the difference in the analytical method employed to evaluate the band-gap values. The band gaps of solids are frequently determined to be different, even for the same nominal composition, depending on the sample type, optical characterization technique, and band-gap assessment method.[14] The band-gap values of solids can be estimated by extrapolating the spectral absorption edge to zero absorbance level, but usually the absorbance spectra of the solids are indirectly acquired. For the band-gap values in Figure 1, the absorbance data for powder $Zn_{1-x}Mg_xO$ were retrieved from diffuse reflectance,[22] while the published data for thin-film $Zn_{1-x}Mg_xO$ were obtained from transmittance measurements.[17]

As described in what follows, cation substitution allows direct control of the optical band gap of ZnO to a certain extent. However, it is of further interest to examine how the detailed optical properties evolve. For the $Zn_{1-x}Mg_xO$ system as an example, we investigated the optical and structural defects induced in the course of cation substitution by the measurement of diffuse reflectance, PL, powder X-ray diffraction, and scanning electron microscopy (SEM). We used polycrystalline $Zn_{1-x}Mg_xO$ (x = 0, 0.05, 0.10, and 0.15) samples prepared by the 550 °C decomposition of mixed oxalates obtained from coprecipitation.[21,22] The cation compositions of the $Zn_{1-x}Mg_xO$ (x = 0.05, 0.10, and 0.15) have been determined as $Zn_{0.950(1)}Mg_{0.050(1)}O$, $Zn_{0.899(1)}Mg_{0.101(1)}O$, and $Zn_{0.850(1)}Mg_{0.150(1)}O$ by Rietveld refinement.[21] Compared with other conventional solid-state reactions and thin-film growth techniques, the present synthesis procedure has several merits. Oxalate formation enables a homogeneous mixing of reactants at the atomic level. Because the oxalate does not contain C−H bonds, precursor decomposition can

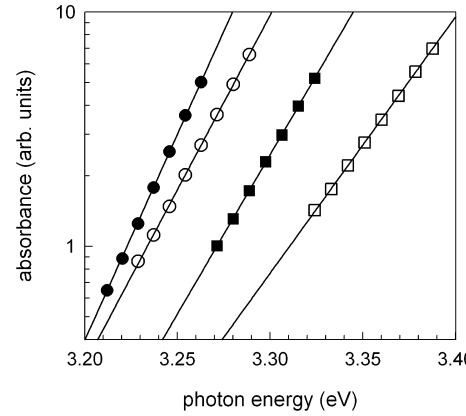

Figure 4. Plot of log A vs $h\nu$ near the absorption edge for $Zn_{1-x}Mg_xO$, where x = 0 (filled circles), 0.05 (open circles), 0.10 (filled squares), and 0.15 (open squares). Gray lines are the linear fits.

be achieved at low temperatures without leaving organic residue. In addition, while thin films by physical deposition can be strained from heteroepitaxy on different substrates and can contain metastable phases beyond thermodynamic solubility, the polycrystalline samples studied here are expected to be fully equilibrated.

Figure 3 shows the diffuse-reflectance spectra and corresponding Kubelka−Munk function (absorbance)[48] of polycrystalline $Zn_{1-x}Mg_xO$ with x = 0, 0.05, 0.10, and 0.15. In both plots, the absorption edges are blue-shifted with an increase in the Mg content. Mg substitution also results in the broadening of the edge slope, but in any case, the transition appears to occur in a single step indicative of phase uniformity of the samples. In order to closely examine the near-band-edge characteristics of the $Zn_{1-x}Mg_xO$ powders, we use a description by Pankove[49,50] of the absorbance (A) in the near-band-edge region:

$$A \propto \exp\left(\frac{h\nu}{E_0}\right) \quad (1)$$

where E_0 is an empirical parameter having dimensions of energy and describing the width of the localized states in the band gap. The magnitude of E_0 accounts for the effects of all possible defects, point, line, or planar.[49] In Figure 4 are shown the absorbance of $Zn_{1-x}Mg_xO$ in the near-edge region as a function of the incident photon energy. For all compositions, the absorbance shows an exponential dependence in the edge regime, as expected from the Pankove model. As determined from the slope of a linear fit of log A as a function of ν, E_0 widths are 24.7 (x = 0), 29.2 (x = 0.05), 31.9 (x = 0.10), and 39.7 meV (x = 0.15). Clearly, the value E_0 increases with x. Such a change in the band-tail feature points out the role of Mg as the defect generator within the $Zn_{1-x}Mg_xO$ lattice.

(48) Kubelka, P.; Munk, F. *Z. Tech. Phys.* **1931**, *12*, 593.
(49) Pankove, J. I. *Phys. Rev.* **1965**, *140*, A2059.
(50) Kim, Y.-I.; Seshadri, R. *J. Korean Phys. Soc.* **2008**, submitted for publication.

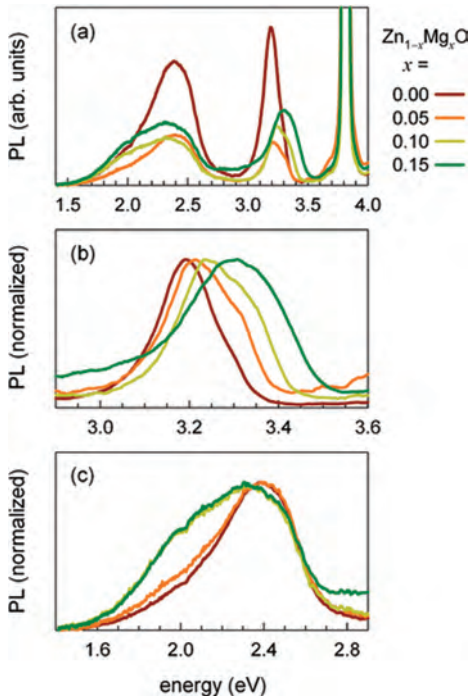

Figure 5. (a) Room temperature PL spectra of polycrystalline $Zn_{1-x}Mg_xO$ excited by a He−Cd laser (3.81 eV) and detailed views of (b) exciton emission and (c) the defect-level emission. In parts b and c, the intensities are normalized to the peak height.

For further optical characterizations of $Zn_{1-x}Mg_xO$ powders, PL spectra were measured using the 325 nm (3.81 eV) line of a He−Cd laser as the excitation source. The PL of ZnO can be divided mainly into two parts: excitonic emission in the UV range and the deep-level defect emissions in the visible range. The green (∼2.4 eV) and yellow (∼2.0 eV) emissions are the most frequent defect emissions from ZnO, while orange-red (∼1.7−1.9 eV) emissions have also been observed occasionally. Although the assignment of the defect emissions to the specific transitions in ZnO is often complicated by the presence of various emission mechanisms, the green emission is generally attributed to the singly ionized O vacancy and/or the Zn interstitial and the yellow emission to interstitial O and/or Zn vacancy.[51–54]

Parts a−c of Figure 5 present the room temperature PL spectra recorded for $Zn_{1-x}Mg_xO$ powders. All of the samples from $x = 0$ to 0.15 clearly exhibit UV excitonic emission between 3.2 and 3.35 eV together with the visible defect emission between 2.0 and 2.4 eV. Exciton emission is the result of electron−hole recombination at the valence/conduction band edges, and therefore its energy directly correlates with the band-gap magnitude. Figure 5b illustrates the blue shift of exciton emission with the Mg content, which confirms the band-gap widening effect of the Mg substitution. For each composition, the peak center of PL emission is slightly (by ∼50 meV) lower in energy than the respective band gap because of a Stokes shift. There is also a significant peak broadening caused by Mg substitution. The peak widths of exciton emission are estimated as 0.16, 0.18, 0.20, and 0.26 eV for $x = 0$, 0.05, 0.10, and 0.15, respectively. Such a peak broadening could arise from compositional fluctuation, which will provide nonuniform Coulomb potentials for the localized excitons.[55] It is expected that $Zn_{1-x}Mg_xO$ possesses large broadening parameters, from the fact that the exciton of ZnO has a small Bohr radius (2.34 nm)[56] and is sensitive to the local inhomogeneity.

The visible PL of $Zn_{1-x}Mg_xO$ powder consists of green (∼2.4 eV) and yellow (∼2.0 eV) emissions, as displayed in Figure 5c. For all of the compositions, the green emission is the dominant component. The intensity of yellow emission is very weak for the samples with $x = 0$ and 0.05 but is markedly enhanced for $x \geq 0.10$. The decomposition of the peak profiles by two-component curve fitting revealed that the positions of both emission bands are nearly independent of the Mg content. Assuming that the green emission is not affected (in both energy and intensity) by the substitution, it is judged that Mg plays a key role in the creation of defect centers for yellow emission. Mg itself may act as the deep-level defect center in the band gap or may stabilize the interstitial O or cation vacancy.

Evolution of Microstructure in $Zn_{1-x}Mg_xO$. In principle, defects associated with some of the optical properties, and structural imperfections, share the same fundamental origin. In this context, the effect of Mg substitution on the microstructure and crystallite morphology was examined by X-ray diffraction line-broadening analysis.[50,57] Powder X-ray diffraction lines are broadened as a result of two types of nonideality in the diffraction experiment: the instrumental limitation and finite crystallinity of the sample.[57] The latter consists of the diffraction-order-independent (size) and diffraction-order-dependent (strain) broadening components in reciprocal space. Most commonly, the size-strain X-ray line-broadening analysis can be carried out in the following steps; (i) estimation of instrumental broadening as a function of 2θ as measured from a reference material, (ii) determination of the diffraction peak widths and positions for the sample to be analyzed, (iii) subtraction of the instrumental broadening from the breadth of the sample data, and (iv) examination of the line-broadening characteristics with respect to the 2θ magnitude.

Using powder X-ray diffraction profiles of $Zn_{1-x}Mg_xO$ powder samples collected at $2\theta = 20-120°$ ($\lambda = 1.5406$ Å), Williamson−Hall (W−H) plots[58] were constructed based on the following relation:

$$\beta_i \cos \theta_i = \frac{\lambda}{D_v} + 4\varepsilon \sin \theta_i \qquad (2)$$

where β_i is the integral breadth (in radians 2θ) of the ith Bragg reflection positioned at $2\theta_i$. The slope and the ordinate

(51) Vanheusden, K.; Warren, W. L.; Seager, C. H.; Tallant, D. R.; Voigt, J. A.; Gnage, B. E. *J. Appl. Phys.* **1996**, *79*, 7983.
(52) Wen, F.; Li, W.; Moon, J.-H.; Kim, J. H. *Solid State Commun.* **2005**, *135*, 34.
(53) Djurisic, A. B.; Leung, Y. H.; Tam, K. H.; Ding, L.; Ge, W. K.; Chen, H. Y.; Gwo, S. *Appl. Phys. Lett.* **2006**, *88*, 103107.
(54) Ramanachalam, M. S.; Rohatgi, A.; Carter, W. B.; Schaffer, J. P.; Gupta, T. K. *J. Electron. Mater.* **1995**, *24*, 413.
(55) Zimmermann, R. *J. Cryst. Growth* **1990**, *101*, 346.
(56) Senger, R. T.; Baraj, K. K. *Phys. Rev. B* **2003**, *68*, 045313.
(57) Snyder, R. L.; Fiala, J.; Bunge, H. J. *Defect and Microstructure Analysis by Diffraction*; Oxford University Press: Oxford, U.K., 1999.
(58) Williamson, G. K.; Hall, W. H. *Acta Metall.* **1953**, *1*, 22.

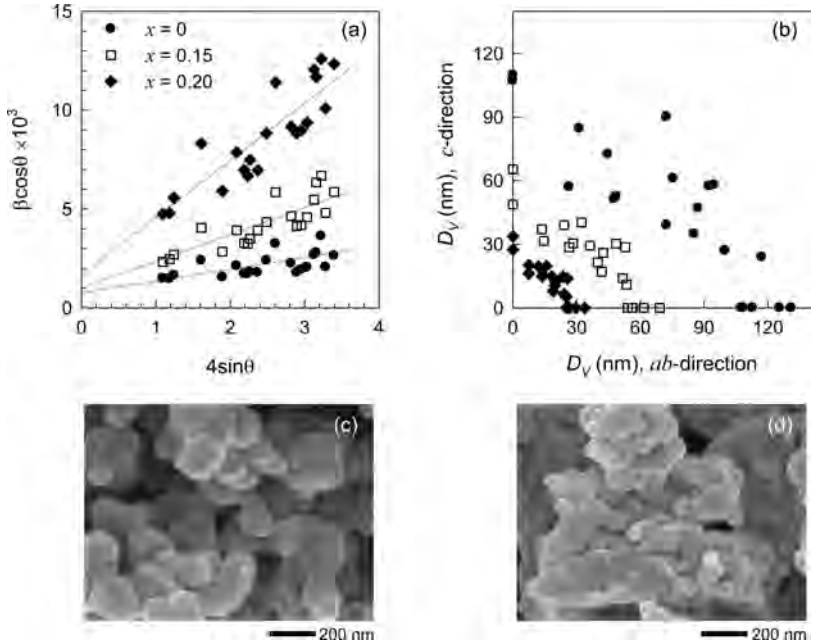

Figure 6. (a) W−H plots and (b) polar diagrams of the apparent crystallite size D_v for ZnO (filled circles), $Zn_{0.85}Mg_{0.15}O$ (open squares), and $Zn_{0.80}Mg_{0.20}O$ (filled diamonds) and corresponding SEM images of (c) ZnO and (d) $Zn_{0.85}Mg_{0.15}O$.

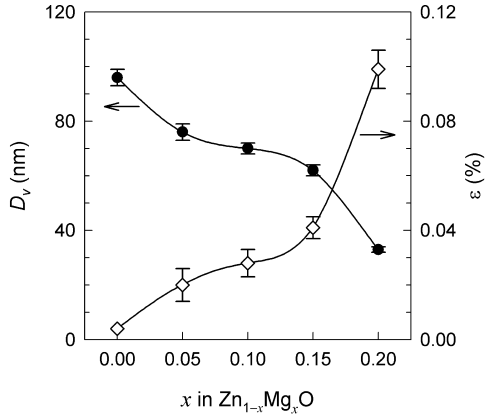

Figure 7. Crystallite size D_v (filled circles) and strain ε (open diamonds) of $Zn_{1-x}Mg_xO$ as determined by the X-ray line-broadening analysis using the simplified integral method. Error bars indicate one estimated standard deviation, and solid lines are guides to the eye.

intercept of the W−H plot can be used to separately estimate the crystallite size (D_v) and strain (ε) contributions to the peak broadening. In Figure 6a, the W−H plots for $Zn_{1-x}Mg_xO$ with $x = 0$, 0.15, and 0.20 are shown. The samples with $x = 0.05$ and 0.10 exhibited line-broadening behavior intermediate between those with $x = 0$ and 0.15. It is observed that the data points on each W−H plot are more or less scattered around a mean straight line, but there is a clear trend of X-ray peak broadening with Mg substitution. Careful investigation of ZnO data reveals that the 00*l* and *h*00 type peak groups have much narrower widths than the *h*0*l* ones. In fact, the uniaxial (00*l* and *h*00) and the off-axial (*h*0*l*) diffraction peak groups fall on their own straight lines. They have different slopes but nearly the same intercept, implying that the ZnO crystallites are fairly isotropic but have a considerable number of stacking faults. The polar diagrams in Figure 6b illustrate the crystallite dimensions along different crystallographic directions. In common for the three samples, D_v is largest along the *h*00, *hk*0, and 00*l* directions and becomes smaller in the *hkl* and *h*0*l* directions. However, there is no significant anisotropic line broadening from either ZnO or $Zn_{1-x}Mg_xO$ ($x > 0$), indicative of the random Mg distribution in $Zn_{1-x}Mg_xO$ with no evidence for Mg clustering.

Parts c and d of Figure 6 present SEM images of ZnO and $Zn_{0.85}Mg_{0.15}O$, respectively. In agreement with the interpretation of the W−H plots, the SEM images reveal that Mg incorporation decreases the crystallite size while maintaining the isotropic grain shape. The results of the X-ray line-broadening analysis for $Zn_{1-x}Mg_xO$ powders are summarized in Figure 7. Evidently, Mg substitution in ZnO reduces the coherent X-ray crystallite size and at the same time introduces microstrain in the wurtzite lattice. The partial replacement of Zn by Mg will inevitably affect the lattice periodicity to induce the internal lattice strain in the individual crystallites and, in turn, suppress grain growth. It is noted that changes of size and strain are somewhat pronounced in the initial and final stages of Mg substitution, which can be ascribed to the microstructural transitions during the gradual Mg incorporation. In the regime of $x < 0.05$, the ZnO lattice undergoes onset of a pseudoternary solid solution. On the other hand, when $x > 0.15$, the solid solution crosses the solubility limit. In other words, the phases with $x = 0$ and 0.20 represent the morphological characteristics at the solubility limits: pure ZnO and the Mg-saturated $Zn_{1-x}Mg_xO$, respectively. On the basis of X-ray line-broadening analysis, we can deduce that the defect characteristics observed in the optical properties of $Zn_{1-x}Mg_xO$ (broader absorption edges and wider exciton emission peaks) mainly stem from the increased surface area and also from the lattice strain imposed by the irregular atomic arrangements.

Summary

The band gap of ZnO can be systematically modulated by the substitution of divalent cations for Zn. The solid solution $Zn_{1-x}Cd_xO$ has narrower band gaps than ZnO, while $Zn_{1-x}Mg_xO$ and $Zn_{1-x}Be_xO$ have wider gaps. By the appropriate choices of substituent cation M (from Be, Mg, and Cd) and its concentration x, the band gap of $Zn_{1-x}M_xO$ can be varied between 3.0 and 3.7 eV. Such a wide range of band-gap tunability presents great promise for the fabrication of desirable barrier layers and quantum-well structures in ZnO-based optoelectronic devices. For the example of the $Zn_{1-x}Mg_xO$ system, it is shown that both structural and optical defects increase with the progress of cation substitution. The distinct coordination preferences of Zn and Mg result in a substantial amount of strain in the solid solution phases. It is suggested that lattice strain leads to reduced crystallite size and eventually dictates the solubility limit. In parallel with the accumulation of structural defects and lattice strain, optical defects of $Zn_{1-x}Mg_xO$ become more pronounced in the band-gap transitions. Strong enhancement of the yellow luminescence is observed for $Zn_{1-x}Mg_xO$ phases with $x \geq 0.10$. Considering the structural similarities between cation components, $Zn_{1-x}Cd_xO$ and $Zn_{1-x}Be_xO$ systems are expected to experience a greater extent of size reduction and lattice strain than $Zn_{1-x}Mg_xO$ with the same x.

Acknowledgment. We gratefully acknowledge support from the National Science Foundation through the MRSEC program (Grant DMR05-20415).

IC800916A